remote sensing

MDPI

Article

Combining LSTM and PLUS Models to Predict Future Urban Land Use and Land Cover Change: A Case in Dongying City, China

Xin Zhao [1], Ping Wang [2,*], Songhe Gao [3], Muhammad Yasir [4] and Qamar Ul Islam [5]

[1] College of Resources, Shandong University of Science and Technology, Tai'an 271000, China
[2] College of Geodesy and Geomatics, Shandong University of Science and Technology, Qingdao 266590, China
[3] Beijing Yuhang Intelligent Technology Co., Ltd., Beijing 100000, China
[4] College of Oceanography and Space Informatics, China University of Petroleum (East China), Qingdao 266580, China
[5] Department of Electrical and Computer Engineering, College of Engineering, Dhofar University, Salalah, 211, Oman
* Correspondence: skd990058@sdust.edu.cn

Abstract: Land use is a process that turns a piece of land's natural ecosystem into an artificial one. The mix of plant and man-made covers on the Earth's surface is known as land cover. Land use is the primary external force behind change in land cover, and land cover has an impact on how land use is carried out, resulting in a synergistic interaction between the two at the Earth's surface. In China's Shandong Peninsula city cluster, Dongying is a significant coastal port city. It serves as the administrative hub for the Yellow River Delta and is situated in Shandong Province, China's northeast. The changes in its urban land use and land cover in the future are crucial to understanding. This research suggests a prediction approach that combines a patch-generation land use simulation (PLUS) model and long-term short-term memory (LSTM) deep learning algorithm to increase the accuracy of predictions of future land use and land cover. The effectiveness of the new method is demonstrated by the fact that the average inaccuracy of simulating any sort of land use in 2020 is around 5.34%. From 2020 to 2030, 361.41 km^2 of construction land is converted to cropland, and 424.11 km^2 of cropland is converted to water. The conversion areas between water and unused land and cropland are 211.47 km^2 and 148.42 km^2, respectively. The area of construction land and cropland will decrease by 8.38% and 3.64%, respectively, while the area of unused land, water, and grassland will increase by 5.53%, 2.44%, and 0.78%, respectively.

Keywords: LUCC; PLUS; LSTM; deep learning; multi-scenario simulation

Citation: Zhao, X.; Wang, P.; Gao, S.; Yasir, M.; Islam, Q.U. Combining LSTM and PLUS Models to Predict Future Urban Land Use and Land Cover Change: A Case in Dongying City, China. *Remote Sens.* **2023**, *15*, 2370. https://doi.org/10.3390/rs15092370

Academic Editor: Bruce D. Chapman

Received: 12 April 2023
Revised: 27 April 2023
Accepted: 28 April 2023
Published: 30 April 2023

1. Introduction

Land Use and Land Cover Change (LUCC) is an important connection between human activities and the natural environment. The rules of land use transformation indicate the interaction between the Earth's environment system on which human beings rely for survival and the increasingly developed production system [1,2]. Modeling research is a core and important component of land change research and is the main way and means to address land usage alteration and other related mechanisms. The model research can replicate and analyze more precisely the geographical and temporal changes in land utilization and land cover change, the pattern and its evolution process, and anticipate the future change trend of key areas [3,4]. There are several models for change simulation that are employed, including dynamic, statistical, and machine learning (ML) models, to suit the high performance needs of land use modeling [5]. In order to objectively track any changes in land use, remote sensing (RS) can capture and evaluate multi-temporal satellite imagery. Data can be stored, processed, and analyzed using Geographic Information

System (GIS), and some land use analysis and simulation models can be programmed directly into GIS software. In the majority of investigations, RS and GIS can be employed alone or together [6–9]. The main models used for early land-use change prediction are the Markov chain model (MC) [10], conversion of land use and its effects (CLUE) [11], cellular automata (CA) model [12], slope, land use, exclusion, urban extension, transportation and hill shade model (SLEUTH) [13], logistic regression (LR) modeling [14], CA–Markov model [15], land transformation model (LTM) [16], land change modeler (LCM) [17], future land use simulation model (FLUS) [18]. Moreover, artificial neural networks and dynamic models are coupled to anticipate land use change [19] and weight of evidence (WOE) is utilized to quantitatively evaluate the driving force of land change [20,21]. To simulate and forecast future land use change, support vector machines are employed to build probability maps [22], among others [23–34].

The patch-generating land use simulation (PLUS) model, which combines a CA framework constructed using multiple types of irregular patch seeds with a land enlargement analytical technique, was initially envisioned in 2021 [35]. This model is more accurate in its simulations and is more in line with the landscape pattern index of the actual terrain when contrasted with prior CA frameworks [35]. To date, many scholars have made various applications based on the PLUS model. Lu et al. [36] used the PLUS model to mimic the geospatial structure of the lower Yellow River at different stages of future development. Lin et al. [37] used the Fuxian Lake basin as an example to incorporate the constrained territory of LUCC and investigate the optimum model for replicating LUCC in this basin utilizing CA–Markov, FLUS, and models. Bao et al. [38] predicted quantitative and spatial variation by coupling MC and analysis of different scenarios. The PLUS-UGB model was developed by Yang Wenjie et al. [39] based on their analysis of the spatial distribution aspects of alterations in land use in Guangzhou. Gao et al. [40] employed the PLUS model to recreate the land utilization data for Nanjing in 2025 under four scenarios and assess changes in various categories of land and land transfers under various scenarios. The numerical composition and spatial organization of production–living–ecological land were refined by Li et al. [41] using a genetic algorithm (GA). To evaluate the models' accuracy, Wang et al. [42] examined PLUS, FLUS, and MC predictions, and the PLUS model was found to be the most efficient for the 2030 terrestrial utilization study.

There are more studies related to land use simulation based on PLUS; however, the methods are mostly based on model coupling and multi-scenario design, without involving deep learning methods. This work enhances the PLUS model by predicting land utilization desire using the long short-term memory (LSTM) technique, taking into account that shifting land use is a complicated process and the trend of future land use is not stable. A type of neural network used to process sequence data is an LSTM network in deep learning models [43]. When faced with extended sequences of data, Recurrent Neural Network (RNN) can only acquire information from the next episode and lacks cognitive performance for the older period, which results in information loss [44]. LSTM is applied to the anticipated demand for land use in this research area and has made some research achievements in land use-related aspects. Xu et al. [45] used MLP and LSTM artificial neural networks as simulation models for comparison. Due to its capacity to capture more time information, LSTM outperforms MLP in modeling the dynamics of urban growth. Boulila et al. [46] realized urban expansion prediction by using the CNN-LSTM network. Wang et al. [47] developed a two-way short-term memory network-based long-time series categorization data gathering model for land use and cover. Mohanrajan et al. [48] developed a bidirectional long- and short-term memory model based on a novel visual transformer for predicting land use/land cover shifts for forested and non-forested areas in the Java Mountains, India.

The PLUS model for land use simulation requires obtaining the land development probability in the land use expansion analysis strategy and setting various parameters such as predicting land use demand in the CA model based on multiple types of random patch seeds to obtain simulation results. The quantity of land use demand has an important

impact on the results of simulation forecasting; therefore, choosing the appropriate land use demand forecasting algorithm is a key step. Using conventional land use demand forecasting algorithms, such as Markov chain, linear regression method, etc., the simulation results are not accurate. Therefore, this paper introduces LSTM, a very popular model in the field of deep learning, to predict the quantity of land use demand based on time series data, which improves the simulation accuracy of the PLUS model.

Dongying is named one of the first international wetland cities, an essential element of the development plan of the Yellow River Delta Efficient Ecological Economic Zone, and the only city where the two national strategies of Yellow and Blue overlap and integrate. Understanding the regional variations in land use is vital so that sustainable development measures can be sought on this basis and ensure the coordinated growth of the economy and the environment. There may be several possibilities for the development of the future pattern of land utilization in Dongying, depending on the regional development strategy.

Taking Dongying City as the research area, this paper formulates a multi-scenario simulation scheme for land use based on the PLUS model and LSTM network to study land use evolution, which provides a variety of decision-making ideas for land resources management and helps to realize the optimal allocation of land resources. The objectives of this study include: (1) LSTM algorithm based on PyTorch deep learning framework to achieve land use demand forecasting, and (2) simulation of future land use in Dongying city under two different scenarios of natural development and ecological development priority.

2. Study Area

The capital of the Yellow River Delta in China is Dongying, a prefecture-level city in Shandong Province. The study area includes two counties (Lijin and Guangrao) and three districts (Hekou, Kenli, and Dongying) under the jurisdiction of Dongying. It lies between 36°55′ to 38°10′N and 118°07′ to 119°10′E in northern Shandong Province. It is adjacent to the Bohai Sea in the east and north, Binzhou in the west, and Zibo and Weifang in the south. The maximum vertical distance from north to south is 123 km, the maximum horizontal distance from east to west is 74 km, and the total land area is 8243 km^2 (see Figure 1).

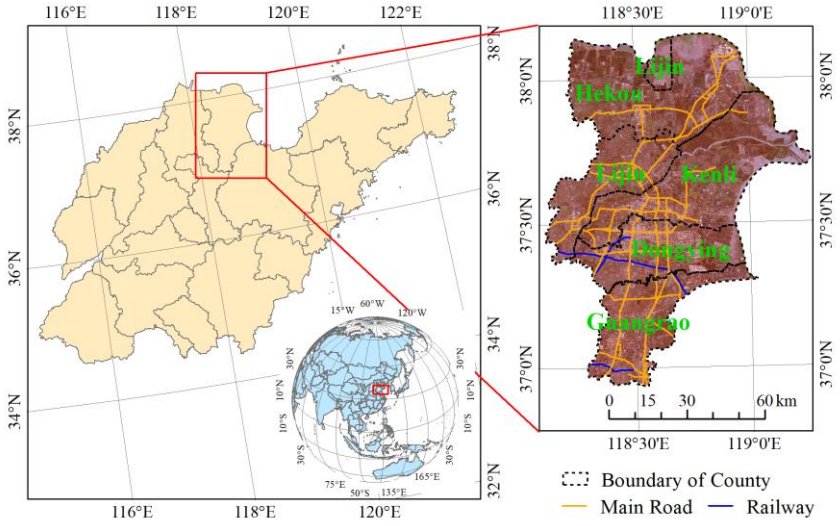

Figure 1. Location of the study area.

3. Material and Methods

3.1. Data Acquisition

China Land Cover Dataset (CLCD) is the first yearly dataset of China's land cover created by Wuhan University using the Google Earth Engine (GEE) infrastructure. The accuracy rate of the CLCD dataset was 79.31%, which was greater than the mean accuracy of the MCD12Q1 and ESACCI LC FROM the GLC and GlobalLand30 datasets [49].

Five sub-regions in the study area based on ArcGIS were randomly chosen for validation, with roughly 6000 sampling points in each area. The overall correct rate could essentially reach about 76%, and sampling results were compared with outcomes of the second national land survey to conclude that CLCD could essentially meet the accuracy requirements of the study area. The projection coordinate system was defined by ArcGIS as WGS_1984_UTM_Zone_50N, and the coordinate system for projection was Universal Transverse Mercartor Grid System (UTM) projection with 6-degree division, and the data of each year were obtained by using vector data masks. On this basis, the land use data of the study area were reclassified into cropland, grassland, water, unused land, and construction land according to the land use types required for this study. Cropland island that is directly or indirectly used for agricultural production. Grassland is the land where herbs and shrubs grow mainly and is suitable for livestock production. Water is rivers, wetlands, etc. Unused land refers to land other than cropland and construction land, mainly including barren land, saline land, swampy land, sandy land, bare land, bare rock, etc. Construction land refers to the land for building and structures, which is land for urban and rural housing and public facilities, industrial and mining land, land for energy, transportation, water conservancy, communication and other infrastructure, tourism land, military land, etc.

The kind of land use changed significantly between 2000 and 2020. (see Table 1 and Figure 2). Cropland in the research region has been gradually shrinking from 5295.27 km^2 to 4423.94 km^2 between 2000 and 2020. The amount of grassland and unused land has decreased at a rate equal to that of cropland, from 1.1% to 0.1% for grassland and from 12.1% to 2.5% for unused land, respectively, a decline of 77.39 km^2 and 712.51 km^2. Contrarily, the area of water and construction land is growing year after year, with the water growing from 282.37 km^2 to 941.94 km^2 or 3.8% to 12.7% of the total, and the construction land growing the highest, from 876.37 km^2 to 1878.03 km^2, or 11.8% to 12.7% of the total. The percentage grew between 11.8% and 25.2%. A total of 1073.93 km^2 and 735.18 km^2 of land were be converted into construction land and water, respectively, from 2000 to 2020. Of these, 678.65 km^2 and 350.76 km^2 of cropland and unused land, respectively, were be converted into construction land, making up 95.9% of the total area converted into construction land. The area of cropland and unused land converted to water is 347.81 km^2 and 304.91 km^2, respectively, accounting for 88.8% of the total area converted to water.

Table 1. Transfer matrix from 2000 to 2020 (km^2).

Land Type	Cropland	Grassland	Water	Unused Land	Construction Land
Cropland	4290.78	4.17	304.91	16.76	678.65
Grassland	39.51	4.47	15.57	4.92	22.16
Water	46.93	0.05	206.77	6.23	22.36
Unused land	45.11	0.53	347.81	153.98	350.76
Construction Land	1.59	0.01	66.89	3.79	804.10

The geographic coordinate system GCS Krasovsky 1940 (Krasovsky 1940 ellipsoid) and the projection Krasovsky 1940 Albers were used to create the vector data for Dongying, which were collected from the Resource and Environment Data Center of the Chinese Academy of Sciences (https://www.resdc.cn/, accessed on 1 September 2022). By specifying the projection with ArcGIS tools, the vector data were defined as the projection coordinate system WGS 1984 UTM_ Zone 50N.

Alteration in LUCC is influenced by several things. In general, the three main forces driving LUCC change are natural, socioeconomic, and accessible considerations. As indicated in Table 2, the PLUS model may investigate the various causes of land use change as well as the contribution of each influencing element to the growth and alteration of each category. In consideration of natural factors, 11 driving factors are selected: slope, aspect, soil erosion, digital elevation model (DEM), average annual temperature, annual accumulated temperature, annual precipitation, moisture index, aridity, net primary production (NPP), and soil organic carbon. These factors are based on various functions of

land resources and are the most fundamental factors for driving force consideration. Many geographic regions have varied patterns of land use, and different elements of nature give diverse impetuses for land use change. This study region is a plain location with flat terrain, and the land is better suited for cultivating crops. This impacts how land is developed and used. The terrain and soil characteristics have a significant impact on the distribution of industrial land used for agriculture, forestry, animal husbandry, and fisheries since they can, to some extent, represent how easily different land resources can be used in the area. The degree of soil erosion and irrigation conditions both reflect the effects of the slope. Unreasonable water and soil resource use causes secondary salinization of the land, which raises groundwater levels and accelerates the destruction of the local biological environment. There is no virtuous cycle since soil erosion, frequent droughts, and flood disasters cause grassland, forest land, and water areas to alter often. Land use may also be influenced by DEM and other statistical indicators of terrain.

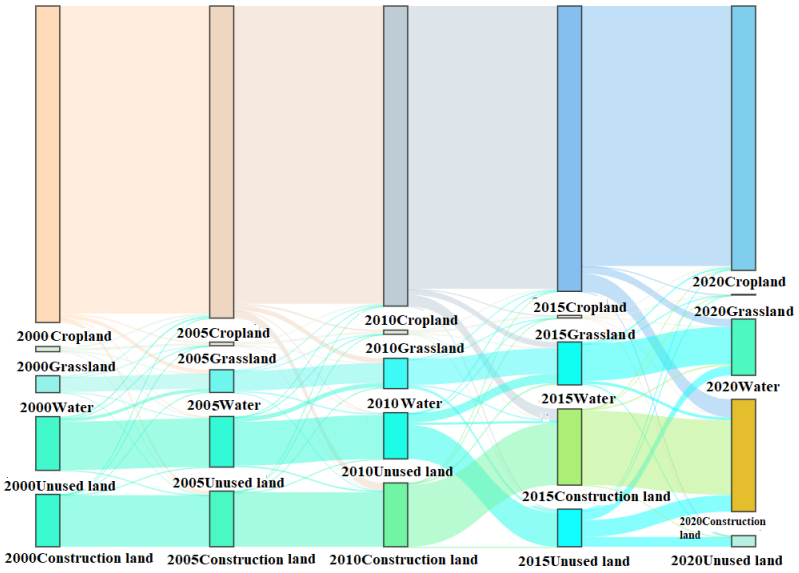

Figure 2. Dongying city 2000–2020 circulation map of various categories.

Gross domestic product (GDP) and population density are the major selection criteria when taking into account social and economic considerations. The interaction between people and society has an impact on how intensively land is used. Humans use land as a means of transportation for a variety of activities carried out in the social context. Social variables will have an impact on human behavior, and behavior, in turn, will have an impact on land use. At the end of 2000, the total population of Dongying was 1,721,300, of which 1,095,500 were involved in agriculture and 711,800 were involved in non-agricultural activities. In 2000–2020, the total population increased from 1,720,000 to 2,190,000, an increase of 27.3%, while the urban population increased from 710,000 to 1,560,000, an increase of 119.7%, a rapid increase, and the city began to enter a phase of rapid urbanization. The study area's urban population started to increase quickly, and the demand for better living conditions and environments encouraged the conversion of agricultural land to construction land, which resulted in a steady loss of agricultural land area. The need for food will rise in tandem with the increase in population density, which will cause unused land, grassland, and other land use types to be converted back into agricultural land. Socioeconomic variables show how human actions have affected the production economy. The rapid economic expansion caused by human output and social activity will further the growth of human activities.

Table 2. Drive factor data and sources.

Data Type	Data Name	Sources
Natural factors	Slope	Original acquisition
	Aspect	Original acquisition
	Soil erosion	http://www.resdc.cn
	DEM	https://earthdata.nasa.gov/
	Average annual temperature	http://www.resdc.cn
	Annual accumulated temperature	http://www.resdc.cn
	Annual precipitation	http://www.resdc.cn
	Moisture index	http://www.resdc.cn
	Aridity	http://www.resdc.cn
	NPP	https://lpdaac.usgs.gov/
	Soil organic carbon	https://data.isric.org/
Social and economic factors	population density	http://www.resdc.cn
	GDP	http://www.resdc.cn
Accessibility factors	Adjacent to highways	Euclidean distance
	Adjacent to railways	Euclidean distance
	Adjacent to water	Euclidean distance
	Adjacent to government	Euclidean distance
	Adjacent to roads I (Multilane road)	Euclidean distance
	Adjacent to roads II (Two-lane road)	Euclidean distance
	Adjacent to roads III (Mixed driving two-lane road)	Euclidean distance
	Adjacent to roads IV (Mixed two-lane or single-lane road)	Euclidean distance

Eight accessibility drivers—including proximity to roads I through IV, proximity to highways, trains, water, and government—were culled to assess the extent of their impact on land use change. The drive factor data must be combined with projection coordinate system UTM, WGS-84 geographic coordinate system, and 30 m resolution resampling. DEM estimated the slope and slope direction. Euclidean distances were calculated for impact factors such as major roads, railways, highways, water, and government distances using the spatial processing tools in ArcGIS. All driving factors were uniformly row-counted and column-counted and made the same as the land extension map.

3.2. Methodology

3.2.1. Research Framework

Figure 3 shows the workflow of this study. The flowchart is composed of three primary modules: first, the LEAS module. Utilizing a random forest to mine the effect of each driver on the growth of geographical units and produce a probability map of the development of each land use in space. This module explores the relationship between each land type and multiple drivers to uncover the conversion rules for each land type; therefore, the results of this module will indicate the development potential of each land type. Second, the CARS module. In order to simulate the evolution of multiple land use types, the CARS module incorporates a stochastic patch generation and a descending threshold mechanism to perform future site simulation based on the traditional CA model. This mechanism generates "seeds" for the development probability of each land use type when the neighborhood effect of the individual land use type equals zero. With the development probability constraint, PLUS will automatically generate the simulated patches. During the simulation, the land use demand will influence the local land use competition pattern through adaptive inertia mechanism, driving the amount of land use to meet the future demand. Using the 2010 data as the initial data, set important parameters such as spatial policy restricted area, land use requirement, transformation regulations, and neighborhood weights for the likelihood of development, and simulate the 2020 land use data. Third,

model accuracy evaluation and correction module. Check the simulation results' correctness in 2020 and make any necessary PLUS model modifications.

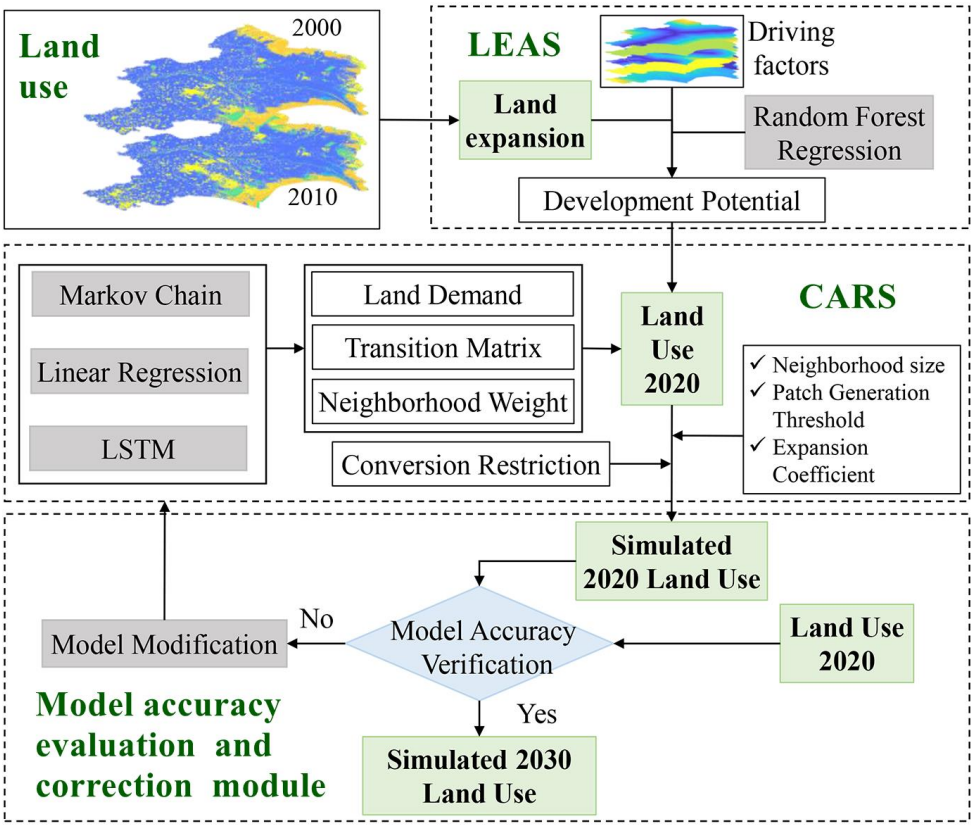

Figure 3. Land use simulation process.

In the CARS module, there are many methods for obtaining land use needs, including the conventional Markov chain and linear regression methods. Experiments have shown that using Markov chains and linear regression to predict the number of land uses in 2020 leads to poor accuracy with the PLUS prediction results compared to the actual land use in 2020. The LSTM deep learning network model, which excels in handling issues that are closely related to time series, is introduced to increase the precision of the PLUS simulation. The land use prediction in 2030 is simulated using the LSTM deep learning network model, which increases the precision of PLUS simulation.

3.2.2. Long Short-Term Memory

Recurrent neural network (RNN) in deep learning models is a class of neural networks dedicated to processing sequential data. RNN can be considered multiple replications of the same neural network, where each neural network module passes the message to the next one. Its input does not only take into account the current data input, but also the input of the previous moments, which together act as the outcome of the present instant, and the outcome of the present instant is not only output but also available for the next moment, which continues to participate in the next moment's output so that the network has a certain memory function. To solve the problem of "long-term dependence", LSTM cells were proposed to improve the memory capacity of standard recurrent cells by introducing "gates" in the cells [50]. Based on the Python environment, PyTorch is used as a deep learning framework to implement the LSTM algorithm. The model uses 5 layers of input and 5 layers of output, the length of the hidden layer output feature vector is 64, and finally, the accuracy is improved using the method of averaging three sets of LSTM results, and the structure diagram is shown in Figure 4. The most important component of the LSTM is the

state cell $s_i^{(t)}$. Here, forget gates are used to manage the self-loop weights (or corresponding time constants) $f_i^{(t)}$, and the sigmoid cell sets the weights to values between 0 and 1.

$$f_i^{(t)} = \sigma\left(b_i^f + \sum_j U_{i,j}^f x_j^{(t)} + \sum_j W_{i,j}^f h_j^{(t-1)}\right) \tag{1}$$

where $x^{(t)}$ is the present input vector, h^t is the present hidden layer vector, and h^t provides the results from each LSTM cell. b^f, U^f, W^f are the bias, input weights, and loop weights of the forgetting gate, respectively. As a result, the internal state of the LSTM cells is updated using a conditional self-loop weight $f_i^{(t)}$ according to Equation (2).

$$s_i^{(t)} = f_i^{(t)} s_i^{(t-1)} + g_i^{(t)} \sigma(b_i + \sum_j U_{i,j} x_j^{(t)} + \sum_j W_{i,j} h_j^{(t-1)}) \tag{2}$$

where b, U, W are the bias in the LSTM cell, the input weights, and the cyclic weights of the forgetting gate, respectively. The external input gate cell $g_i^{(t)}$ is updated similarly to the forgetting gate, but with its parameters.

$$g_i^{(t)} = \sigma(b_i^g + \sum_j U_{i,j}^g x_j^{(t)} + \sum_j W_{i,j}^g h_j^{(t-1)}) \tag{3}$$

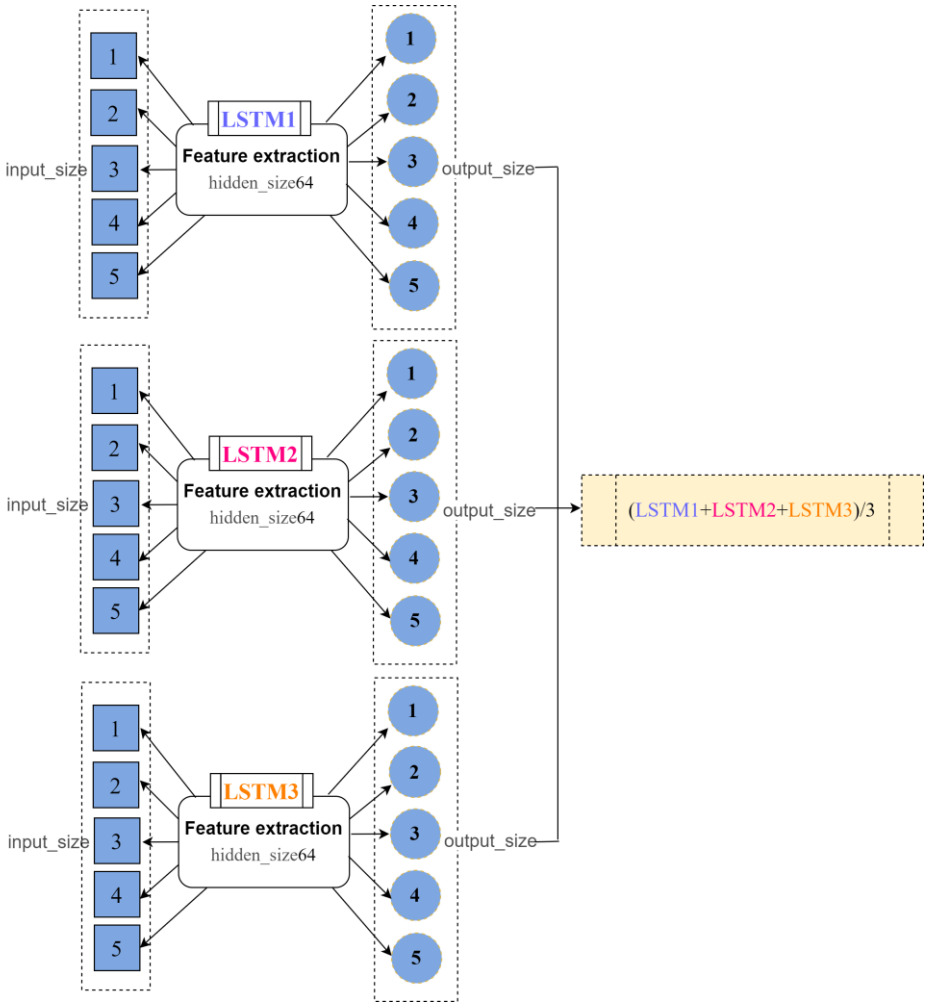

Figure 4. Structure of LSTM prediction method.

The output of the LSTM cell $h_i^{(t)}$ can also be closed by an output gate $q_i^{(t)}$ (using a sigmoid cell as a gate).

$$h_i^{(t)} = \tan h(s_i^{(t)}) q_i^{(t)} \tag{4}$$

$$q_i^{(t)} = \sigma(b_i^o + \sum_j U_{i,j}^o x_j^{(t)} + \sum_j W_{i,j}^o h_j^{(t-1)}) \tag{5}$$

where b^o, U^o, W^o are the bias, input weights, and loop weights of the forgetting gates, respectively. Three gates $s_i^{(t)}$ can be selected as additional inputs to the first cell.

The loss function is employed to quantify the degree to which the model's predicted value deviates from the actual value. Generally speaking, a model performs better the loss function. Loss functions for various models are typically different. mean absolute error loss (also called L_1 loss) and mean squared error loss (also called L_2 loss) are the two loss functions frequently employed in regression issues [51].

3.2.3. Patch-Generating Land Use Simulation Model

A raster-based patch-generating land use simulation model was created to assist in the identification of probable drivers and their various contributions to change, allowing for a better understanding of the relationships underlying LUCC changes. The model contains a brand-new data mining approach for locating land use change laws. To better replicate and model actual landscape patterns, this model combines a CA model with a patch-generating simulation technique [35].

1. *Land expansion analysis strategy*

The random forest classification (RFC) technique is used by LEAS to investigate the connection between changing land use types and various factors. The RFC algorithm is a decision-tree-based integrated classifier that can handle multidimensional input data and output the growth probability $P_{i,j}^d$ of type k at cell i.

$$P_{i,j}^d(x) = \frac{\sum_{n=1}^{M} I(h_n(x) = d)}{M} \tag{6}$$

Other forms of utilization are transformed to type k if the value of d is 1, and other transformations are indicated if it is 0; M is the total number of decision trees, and x is a composite vector of several drivers. $h_n(x)$ is the prediction type of the nth decision tree of vector x.

The LEAS module extracts the ultimate potential growth of each land use in space by analyzing the effects of each driver on the growth of geographic units based on random forests. While ignoring the source type of land use, LEAS can examine the expanding zones of each changing land use to determine the transitional rules for all land use types. By avoiding the analysis of transition types, which increases exponentially with the number of land use types, the analysis process of land use change is effectively simplified.

2. *CA model based on multi-type random patch seeding*

The cellular automata model based on multi-type random patch seeds (CARS) is a model that includes the plaque formation mechanism of random seeds based on multiple land uses. The CA model is a scenario-driven land-use simulation model that integrates "top-down (e.g., global land use demand)" and "bottom-up (e.g., local land-use competition mechanisms)". In the simulation process, the land use demand will affect the local land use competition mode through the adaptive inertia mechanism, driving the amount of land use to meet future demand.

To simulate the evolution of multiple land use types, the CARS module combines random seed generation and a descending threshold to perform future land use simulation operations based on the traditional CA model. When the neighborhood effect of a single land-use type equals 0, the mechanism generates "seeds" to the development probability

of each land-use type. Subject to the development probability, PLUS will automatically generate simulated plaques.

3.2.4. Accuracy Verification

In this study, the superior value FoM is employed to describe the LUCC model's accuracy. The ratio of the intersection of observed and predicted changes to the sum of observed and predicted changes is known as figure of merit (FoM) [52]. The value figure might be between 0% and 100%.

$$FoM = B/(A + B + C + D) \quad (7)$$

where A represents the incorrect region due to observed changes that are predicted to be persistent, B represents the correct region due to observed changes that are predicted to be variable, C represents the incorrect region due to observed changes that are predicted to be incorrectly acquired categories, and D represents the incorrect region due to observed tenacity that is predicted to be variable.

LUCC models with larger variability tend to have higher prediction accuracy and higher FoM. To account for model error, both observed and predicted variation must be considered. The importance of describing map differences based on quantitative inconsistencies and positional inconsistencies. For evaluating the accuracy of simulated variation, the FoM index is superior to the widely used kappa coefficient [53]. It was discovered through validation that FoM index values frequently fall between 0 and 0.59 and are typically lower than 0.3 [18].

4. Results

4.1. Land Use Multi-Scenario Simulation

Scenario simulation analysis is a kind of scenario description of future land use development based on historical data. By presetting different development goals, it simulates the future land use pattern in the study area under different scenarios. For different characteristics of the study area, different scenario simulation analyses can be used to achieve the optimal allocation of land resources and can provide a variety of decision-making thinking on land resource management. Influenced by regional development strategies, there may be multiple possibilities for the evolution of future land use patterns in the Yellow River Delta. Since the Shandong Yellow River Delta National Nature Reserve is divided into two areas, north and south, the southern area is located at the current mouth of the Yellow River and belongs to the Kenli district, while the northern area is located at the mouth of the former Yellow River channel after its diversion in 1976 and belongs to Hekou district. Therefore, ecological development priority scenarios were simulated for the Hekou district and Kenli district, and natural development scenarios were simulated for the Dongying district, Guangrao County and Lijin County.

4.2. PLUS Simulation of Natural Development Scenario

According to the expansion patterns and change characteristics of various land use types in the study area throughout history and following the land use structure change pattern, the natural development scenario takes into account the relationship between natural, socioeconomic, and accessibility factors and land use changes. For Dongying district, Guangrao, and Lijin counties, the number of land demand rasters in 2030 was predicted using LSTM networks based on historical images of land use in 2000 and 2010, and natural development scenarios were simulated for Dongying district, Guangrao, and Lijin county, respectively. Assuming a natural development scenario, Table 3 displays the real land use data for 2020 and the predicted data for 2030.

Table 3. Land use area under natural development scenarios in 2020 and 2030 (km^2).

Land Type	2020 Dongying District	2030 Dongying District	2020 Guangrao County	2030 Guangrao County	2020 Lijin County	2030 Lijin County
Cropland	539.78	481.52	782.60	720.11	897.45	850.63
Grassland	0.78	5.60	0.11	2.64	0.01	0.19
Water	148.24	126.05	77.10	46.31	53.82	51.25
Unused land	34.41	84.15	13.50	47.81	15.00	52.70
Construction Land	423.66	449.55	297.14	353.58	231.51	243.02

In Dongying district, cropland will shrink from 539.78 km^2 to 481.52 km^2 between 2020 and 2030, accounting for 41.98% of the total area instead of 47.06%. From 0.78 km^2 to 5.6 km^2, or 0.07% of the total area, the grassland area rose. From 12.93% of the total area to 10.99%, or 148.24 km^2 to 126.05 km^2, the water area fell. Unused land increased in size from 34.41 km^2 to 84.15 km^2, making up 7.34% of the overall area. Building land expanded from 423.66 km^2 to 449.55 km^2, accounting for 39.2% of the whole area, up from 36.94%. According to a comprehensive analysis, cropland has the biggest change among various land use types, with a decrease of 5.08%. The second is unused land, up 4.34%. Thirdly, construction land increased by 2.28% and water area decreased by 1.94%. The grassland is relatively stable and only increased by 0.42%.

From 2020 to 2030, the cropland area of Guangrao county will decrease from 782.60 km^2 to 720.11 km^2, and the percentage will drop from 66.86% to 61.52% in the overall area. The water area fell from 53.82 km^2 to 51.25 km^2, representing 4.28% of the total area from 4.49%; the grassland area rose from 0.01 km^2 to 0.09 km^2, representing 0.01% of the total area; the undeveloped land rose in size from 15 km^2 to 52.7 km^2, or 4.4% of the total area, up from 1.25%; the construction land expanded from 231.51 km^2 to 243.02 km^2, making up 20.29% of the whole area as opposed to 19.33%. Further analysis revealed that cropland has the biggest change among various land use types, with a decrease of 5.34%. The second is construction land, up 4.82%. Thirdly, the unprofitable land increased by 2.93% and the water area decreased by 2.63%. The grassland is relatively stable and only increases by 0.22%.

The cropland area in Lijin county will drop from 897.45 km^2 to 850.63 km^2 between 2020 and 2030, while its share of the overall area will fall from 74.93% to 71.02%. The area of grassland increased from 0.01 km^2 to 0.09 km^2, making up 0.01% of the overall area; 4.28% of the total area, down from 4.49%, was made up of water, which declined from 53.82 km^2 to 51.25 km^2; From 1.25% to 4.4% of the total area, the amount of undeveloped land expanded from 15 km^2 to 52.7 km^2; construction land expanded from 231.51 km^2 to 243.02 km^2, making up 20.29% of the whole area as opposed to 19.33%. According to a comprehensive analysis, cropland has the biggest change among various land use types, with a decrease of 3.91%. The second is unused land, up 3.15%. Thirdly, construction land increased by 0.96% and water area decreased by 0.21%. The grassland is relatively stable and only increases by 0.01%.

4.3. PLUS Simulation of Ecological Development Priority Scenario

The concept of ecological priority and green development is the basis of the priority ecological development program. While optimizing the pattern of territorial space development and protection, ecological civilization is integrated into the overall process and support level of environmental protection in the Yellow River Delta. The number of land demand rasters for Hekou district and Kenli district in 2030 is estimated using an LSTM network based on historical land use pictures from 2000 to 2010. Table 4 displays the land use outcomes of 2030 ecological development priority scenarios. The ecological source area and high habitat quality area are taken as the ecology preservation restricted area.

Table 4. Land use area under ecological development priority scenarios in 2020 and 2030 (km^2).

Land Type	2020 Hekou District	2030 Hekou District	2020 Kenli District	2030 Kenli District
Cropland	998.44	959.85	1204.68	1140.27
Grassland	0.53	6.66	7.8	51.65
Water	410.83	577.86	251.27	321.63
Unused land	76.79	200.55	45.97	211.74
Construction Land	456.38	198.05	469.46	253.9

To extract the ecological source site, the core area needs to be found. The morphological spatial grid will segment the foreground objects of the input image. The statistical number of core area surface after segmentation is 68,113 rasters, and the core area of the original data is severely fragmented. The statistical area of the core area is sorted from large to small, and the surface with an area larger than 0.7 km^2 is selected and combined and extracted, that is, about 86.56% of the core area is extracted as ecological source land, which greatly reduces the fragmentation degree. This ecological source area is mainly concentrated in the Yellow River Delta Reserve and the Yellow River Estuary Ecotourism Area.

Running the habitat quality module, the degradation degree image was generated for the first time, and the maximum value of degradation was 0.0818, at which time the obtained habitat quality map had an extremely uneven distribution of index values, causing aggregation. Therefore, it is necessary to adjust the habitat parameter to half of the maximum degradation value, i.e., 0.0404, and run the program again to obtain the habitat quality map. The habitat quality values were separated at equal intervals, and the habitat quality was classified into five habitat quality classes: low, lower, medium, higher, and high. Areas with high habitat quality and ecological source sites were taken as ecological development protection sites, i.e., restricted areas under the ecological priority scenario.

Under the priority scenario of ecological development in the Hekou district from 2020 to 2030, the area of cropland decreases from 998.44 km^2 to 959.85 km^2, representing 51.39% to 49.4%. In terms of the percentage of the overall area, grassland grows from 0.53 km^2 to 6.66 km^2, or from 0.03% to 0.34%. Water covered an area that expanded from 410.83 km^2 to 577.86 km^2, or 21.14% to 29.74% of the total area. Unused land increased in size from 76.79 km^2 to 200.55 km^2, or 3.95% to 10.32% of the total area. Construction land's area shrunk from 456.38 km^2 to 198.05 km^2 or 23.49% to 10.2% of the total area. Comprehensive analysis, the biggest change in various land use types is construction land, down 13.29%; followed by water up 8.6%, unused land up 6.37%, cropland down 1.99%, and grassland up 0.31%.

In the Kenli district, cropland will shrink from 1204.68 km^2 to 1140.27 km^2 between 2020 and 2030, and its share of the whole area will drop from 60.87% to 57.61%. In contrast, grassland will grow from 7.8 km^2 to 51.65 km^2, accounting for 2.61% of the total area, up from 0.39%. Water coverage grew from 251.27 km^2 to 321.63 km^2, or 16.25%, from 12.7% of the total area. The area of undeveloped land increased from 45.97 km^2 to 211.74 km^2, or 10.7% of the total area, up from 2.32%. Construction land reduced in size from 469.46 km^2 to 253.9 km^2, accounting for 12.83% of the total area as opposed to 23.72%. According to a thorough investigation, cropland decreased by 3.26%, cropland decreased by 10.89%, cropland increased by 3.26%, grassland increased by 2.22%, unused land increased by 8.38%, water increased by 3.55%, and building land decreased by 10.89%.

4.4. Land Use Conversion from 2020 to 2030

The interaction between different types of land use is intricate and competitive in the land system. As water areas are increased, other land uses must be scaled back, and when biological lands are protected, cropland and construction sites must bear the burden of all development. Therefore, to address the needs of protecting cropland, the environment, and urban co-development, the relevant departments must develop pertinent policies, beginning with sustainable development, and the protection of the ecological

environment must be put in the top priority position to avoid the issue of the ecological environment degrading while the financial and cultural development is going on. To secure the harmonious development of social and economic development and ecological conservation, it is also vital to avoid destroying the current ecological base via the disorderly extension of construction land and to put the protection of cropland into practice.

Figure 5 shows the transition between land-use categories from 2020 to 2030. Figure 6 visualizes the actual and simulated land use distribution in 2020 and 2030. The area of land that will be transferred to water between 2020 and 2030 will be the most, at 613.3 km^2, followed by cropland, unused land, and construction land, at 514.35 km^2, 489.49 km^2, and 391.3 km^2, respectively. The area of land that will be transferred to grassland land will be the least, at 59.47 km^2. The conversion between cropland and water, with an area of 424.11 km^2, followed by the conversion between construction land and cropland, with an area of 361.41 km^2, makes up the majority of the transfer of land use. The remaining land types are primarily concentrated in the conversion between unused land and cropland, with an area of 211.47 km^2 each. The remaining land types are mostly concentrated in the area that results from the transition of cropland, unused land, and water, which is 42.37 km^2, 211.47 km^2, and 148.42 km^2, respectively.

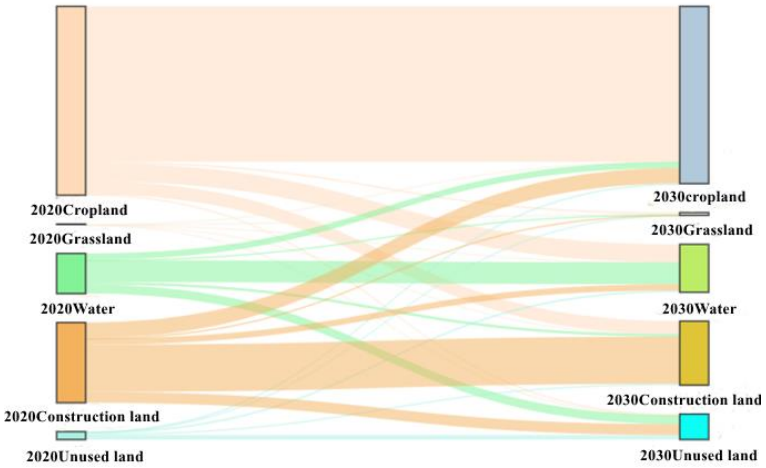

Figure 5. Dongying city 2020–2030 circulation map of various categories.

According to the analysis of the full study region in Figure 6, the cropland area will decrease from 4421.57 km^2 to 4153.08 km^2 from 2020 to 2030, representing 55.83% of the total area from 59.47%. The grassland area increased by 0.9%, from 9.23 km^2 to 66.74 km^2, or 0.12% of the total area. From 12.66% to 15.1% of the total area, the water area rose from 940.97 km^2 to 1123.24 km^2. From 2.5% of the total area to 8.03% of the total area, the unused land area expanded from 185.54 km^2 to 597.05 km^2. The area of construction land decreased from 1877.46 km^2 to 1498.38 km^2, and the proportion in the total area decreased from 25.25% to 20.14%. According to a comprehensive analysis, construction land decreased by 8.38%, unused land increased by 5.53%, cropland decreased by 3.64%, water area increased by 2.44%, and grassland increased by 0.78%.

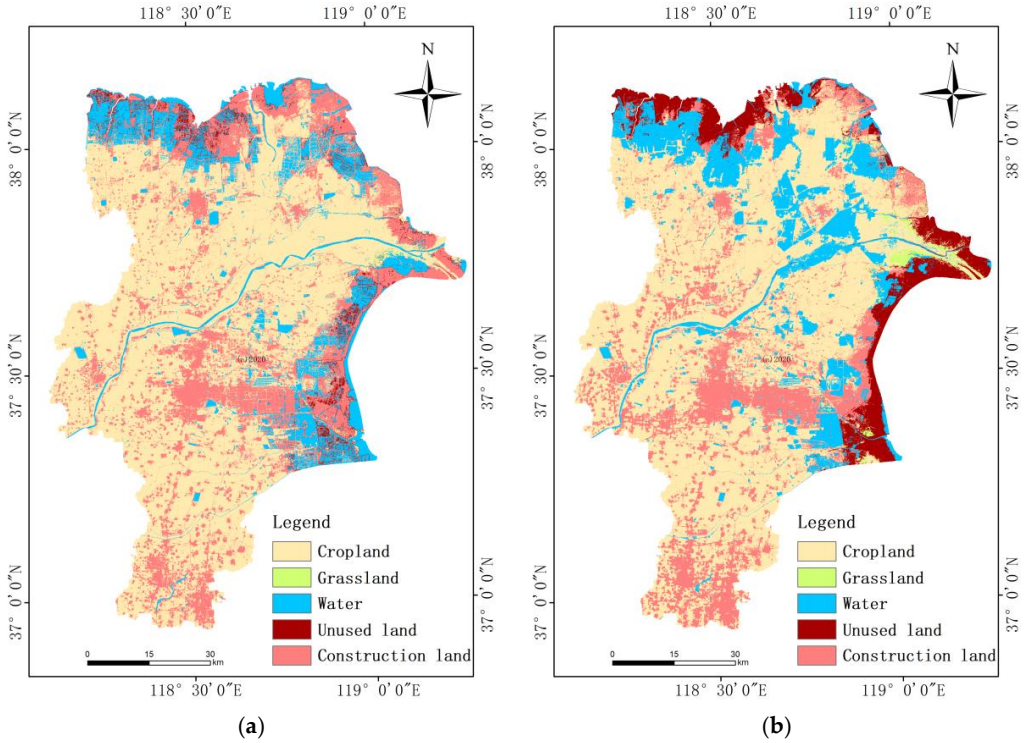

Figure 6. Multi-scenario simulation analysis of land use: (**a**) actual data in 2020; (**b**) simulated data in 2030.

4.5. Contribution of Driving Factors

The LEAS module in the PLUS model employs the random forest model method to determine the likelihood that each type of land use would develop, as well as the role that each driver played in the conversion of that type of land use into another type of land use (see Figure 7). The sampling rate is 0.1, and the number of decision trees is set to 50.

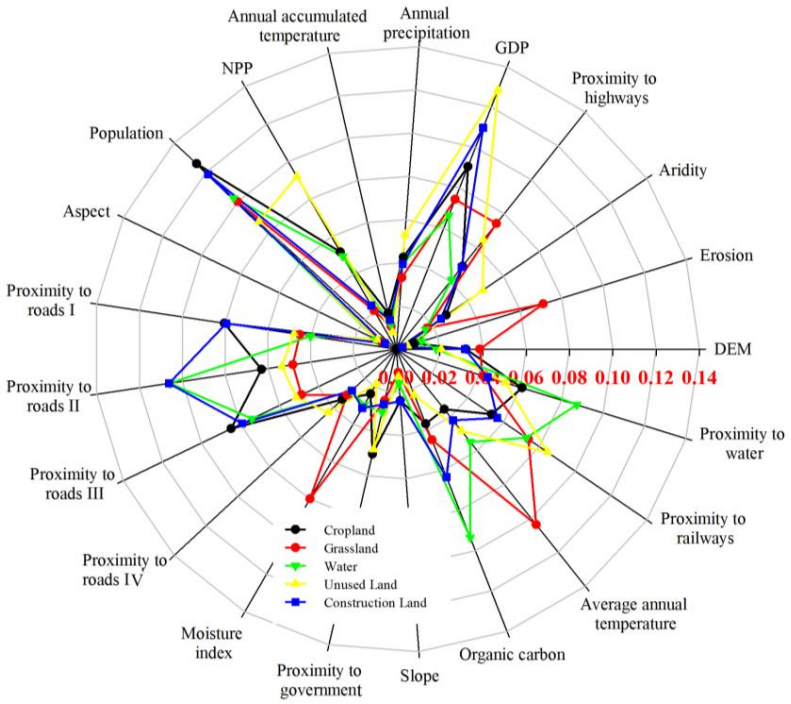

Figure 7. Contribution of driving factors to expansion of various land use.

The driver of the largest contribution to cropland area expansion is population density, followed by GDP and distance to tertiary roads. Roads III is a type of road with a low road surface level, whose main function is to connect local counties, towns and villages, remote suburban areas, or functional area locations. This contribution indicates that the cropland in the study area is closely related to human distribution, which is mostly distributed around rural areas and positively correlated with the distance to tertiary roads while being far from areas with higher GDP. The largest contribution of grassland expansion was the average annual temperature, followed by population density and moisture index. This indicates that the distribution of grasslands is highly correlated with temperature, with suitable temperature and wetness being hot areas for grassland distribution and negatively correlated with population density. The greatest contribution of water area expansion is the distance to secondary roads and population density. Water areas are also closely related to human distribution and are mostly located in less densely populated areas with easy access. The largest expansion of unused land is GDP. Changing land use will change GDP. GDP fluctuates from high to low as an element or asset, showing that a change in land use causes a market value to drop to zero. Population density, GDP, and proximity to secondary roads are the three factors that affect the expansion of construction land the most. According to actual urban development, the majority of construction land is dispersed in regions with high densities of people, businesses, and vehicles. Future construction land will also expand in areas with high population concentration and well-developed transportation arteries.

5. Discussion

5.1. Uniqueness of the Study Area

The Yellow River Delta is rich in natural resources and intact ecosystems, carrying a major mission of national environmental and energy security, and harboring huge potential for economic growth. However, the accelerated urbanization and increasingly frequent human activities in recent years have led to the intensification of wetland landscape fragmentation, biodiversity reduction, and environmental pollution, which, together with the reduction in incoming sediment, soil salinization, and wetland ecosystem reverse succession, have made the originally fragile and sensitive ecosystem of the Yellow River Delta face serious challenges and pose a significant risk to the region's ability to sustain its development. It seriously jeopardizes the region's ability to develop economically and socially sustainably. In this context, the possible future land use scenarios of the Yellow River Delta are simulated and predicted based on the PLUS model using the LSTM network, which is important for reconciling the conflicts between conservation and development and formulating scientific regional development plans.

5.2. Improved PLUS Model Based on LSTM

Based on the Python environment, the LSTM algorithm is implemented using Python as a deep learning framework. The model uses 5 layers of input, and 5 layers of output, and the length of the hidden layer output feature vector is 64. Finally, the method of averaging three sets of LSTM results is used to improve accuracy. Set the loss function to which the predicted value and the true value are different, the better the loss function, the better the performance of the model. Different models generally use different loss functions. Mean squared error loss is one of the most commonly used loss functions in machine learning and deep learning regression tasks and is also known as L_2 loss. Mean absolute error is another commonly used loss function, also known as L_1 loss.

FoM values are large for areas with large land use changes. A small land use change leads to a small FoM value. The land use change in Dongying is relatively small; therefore, the overall FoM value is small. Analyze the impact of three different methods of Markov chain, linear regression, and LSTM network in predicting land use demand results on the accuracy of PLUS simulation results in 2020 under the same parameter settings (see Table 5). The results have an overall high accuracy rate, with an average error of about 5.34%,

indicating that the accuracy of the simulation has achieved the desired effect. Cropland has the highest simulation accuracy; grassland and unused land have lower accuracy rates; water and construction land have intermediate accuracy rates. The simulation accuracy increases as the FoM value increases. The maximum simulation accuracy is achieved by the enhanced PLUS model based on the LSTM L_1 Loss network, and the FoM value is 0.1335. The enhancement of the PLUS model based on the LSTM network is effective, according to experiments. For erratic time series with a greater number of fixed components, LSTM networks typically perform better. Since the L_1 Loss function does not depend on the output deviating from the true value, it is more suited to preserving the model's stability. It computes the absolute value of the difference between the estimated value and the true value. To improve precision, three groups of LSTM data are averaged.

Table 5. Comparison of land use PLUS simulation accuracy in 2020.

Prediction Method of Land Use Demand	Markov Chain	Linear Regression	LSTM L_1 Loss	LSTM L_2 Loss
2020FoM	0.0852	0.0928	0.1335	0.1293

From Table 6, it can be seen that the overall accuracy of the simulation of the PLUS improved model based on the LSTM network is high, and the average error is about 5.34%, indicating that the accuracy of the simulation has achieved the desired effect. Among them, the accuracy of cropland simulation is the highest. Grassland and unused land have lower accuracy and the accuracy rate of water and construction land is in the middle.

Table 6. Comparison between simulated area and actual area in 2020.

Number of Land Use Rasters	Cropland	Grassland	Water	Unused Land	Construction Land
Actual number in 2020	4915486	10257	1046601	206312	2086697
MC-based predicts number of simulations	4900257	111142	943662	679400	1645803
LR-based predicts number of simulations	5258616	49011	796388	713674	1345696
LSTM L_1 loss-based predicts number of simulations	4940619	11282	1094461	221467	1997524
Error (%)	0.51%	9.99%	4.57%	7.34%	−4.27%

5.3. Multi-Scenario Analysis

A type of scenario description of future land use development based on historical data is scenario simulation analysis. It stimulates the future land use pattern in the research area under various scenarios by presetting various development targets. Several scenario simulation analyses can be utilized to achieve optimal land resource allocation and can offer a variety of decision-making thoughts on land resource management depending on the characteristics of the studied area. The regional development strategy may have a significant impact on how the Yellow River Delta's future land use pattern develops. Due to the north and south divisions of the Shandong Yellow River Delta National Natural Reserve, the southern area is located at the current mouth of the Yellow River and belongs to the Kenli district, while the northern area is located at the mouth of the old Yellow River channel after its diversion in 1976 and belongs to the Hekou district. Therefore, ecological

development priority scenarios were simulated for Hekou and Kenli districts, and natural development scenarios were simulated for the Dongying districts, Guangrao county, and Lijin county.

6. Conclusions

This study uses a combination of the PLUS model and the LSTM network to predict the land use of different administrative districts in Dongying city in 2030 under different development scenarios. The evolution of land use in Dongying city from 2020 to 2030 is analyzed. Comparing and quantifying the three methods of MC, LR, and LSTM for predicting the quantity of land use demand under the same parameters, the accuracy of PLUS simulation verifies that the precision of the PLUS-enhanced model prediction based on the LSTM network achieves the desired effect.

A simulation of land usage under multiple scenarios (including natural development and ecological development priorities) and a simulation of changes to the environment in 2030 are presented. The cropland area is extensively converted to the construction land area in the Dongying district, Guangrao county, and Lijin county under the natural development scenario, resulting in a significant increase in the construction land area and a decrease in the cropland area of about 167 km^2. However, in Hekou and Kenli districts, the area of cropland and construction land has greatly decreased under the priority scenario of ecological development, while the water area has significantly risen by about 103 km^2. Cropland will be changed to water in an area of 424.11 km^2 and construction land will be converted to cropland in an area of 361.41 km^2 between 2020 and 2030. It can be seen that the sub-regional scenario simulation scheme proposed in this paper can effectively predict future ecological protection and high-quality development in Dongying City.

Dongying City takes a high level of ecological environment protection to promote high-quality economic development as its future goal. How to model and optimize the spatial allocation of land resources in Dongying City based on more accurate multi-scenario models is the focus of future research. Improving the efficiency of land resource allocation and output, promoting the quality of urbanization, and coordinating regional development in China can provide new impetus for the next round of economic growth.

Author Contributions: Conceptualization, X.Z., P.W., S.G. and M.Y.; Methodology, X.Z.; software, S.G.; validation, M.Y. and P.W.; formal analysis, X.Z.; investigation, S.G.; resources, M.Y.; data curation, S.G.; writing—original draft preparation, X.Z. and Q.U.I.; writing—review and editing, P.W. and X.Z.; visualization, M.Y.; supervision, S.G. All authors have read and agreed to the published version of the manuscript.

Funding: This paper is supported by College of Resources, Shandong University of Science and Technology.

Data Availability Statement: All data used during the study are available at https://zenodo.org/record/4417810.

Conflicts of Interest: The authors declare no conflict of interest.

References

1. Brown, D.G.; Walker, R.; Manson, S.; Seto, K. Modeling land use and land cover change. In *Land Change Science: Observing, Monitoring and Understanding Trajectories of Change on the Earth's Surface*; Kluwer Academic Publisher: London, UK, 2004; pp. 395–409. [CrossRef]
2. Ilyasd, M.; Yasir, M.; Hossain, M.S. Urban Area Extraction and Land Use Land Cover Monitoring of Charsadda District, Pakistan. *Earth Sci. Malays. (ESMY)* **2022**, *6*, 96–102. [CrossRef]
3. Baker, W.L. A review of models of landscape change. *Landsc. Ecol.* **1989**, *2*, 111–133. [CrossRef]
4. Lambin, E.F. Modelling and monitoring land-cover change processes in tropical regions. *Prog. Phys. Geogr.* **1997**, *21*, 375–393. [CrossRef]
5. Aburas, M.M.; Ahamad, M.S.S.; Omar, N.Q. Spatio-temporal simulation and prediction of land-use change using conventional and machine learning models: A review. *Environ. Monit. Assess.* **2019**, *191*, 205. [CrossRef]
6. Alghais, N.; Pullar, D. Modelling future impacts of urban development in Kuwait with the use of ABM and GIS. *Trans. GIS* **2018**, *22*, 20–42. [CrossRef]

7. Islam, K.; Jashimuddin, M.; Nath, B.; Nath, T.K. Land use classification and change detection by using multi-temporal remotely sensed imagery: The case of Chunati wildlife sanctuary, Bangladesh. *Egypt. J. Remote Sens. Space Sci.* **2018**, *21*, 37–47. [CrossRef]
8. Ji, W.; Ma, J.; Twibell, R.W.; Underhill, K. Characterizing urban sprawl using multi-stage remote sensing images and landscape metrics. *Comput. Environ. Urban Syst.* **2006**, *30*, 861–879. [CrossRef]
9. Mundia, C.N.; Aniya, M. Analysis of land use/cover changes and urban expansion of Nairobi city using remote sensing and GIS. *Int. J. Remote Sens.* **2005**, *26*, 2831–2849. [CrossRef]
10. Huang, W.; Liu, H.; Luan, Q.; Jiang, Q.; Liu, J.; Liu, H. Detection and prediction of land use change in Beijing based on remote sensing and GIS. *Int. Arch. Photogramm. Remote Sens. Spat. Inf. Sci* **2008**, *37*, 75–82.
11. Liu, M.; Hu, Y.; Chang, Y.; He, X.; Zhang, W. Land use and land cover change analysis and prediction in the upper reaches of the Minjiang River, China. *Environ. Manag.* **2009**, *43*, 899–907. [CrossRef] [PubMed]
12. Araya, Y.H.; Cabral, P. Analysis and modeling of urban land cover change in Setúbal and Sesimbra, Portugal. *Remote Sens.* **2010**, *2*, 1549–1563. [CrossRef]
13. KantaKumar, N.L.; Sawant, N.G.; Kumar, S. Forecasting urban growth based on GIS, RS and SLEUTH model in Pune metropolitan area. *Int. J. Geomat. Geosci.* **2011**, *2*, 568–579.
14. Park, S.; Jeon, S.; Choi, C. Mapping urban growth probability in South Korea: Comparison of frequency ratio, analytic hierarchy process, and logistic regression models and use of the environmental conservation value assessment. *Landsc. Ecol. Eng.* **2012**, *8*, 17–31. [CrossRef]
15. Al-Sharif, A.A.; Pradhan, B. Monitoring and predicting land use change in Tripoli Metropolitan City using an integrated Markov chain and cellular automata models in GIS. *Arab. J. Geosci.* **2014**, *7*, 4291–4301. [CrossRef]
16. Tayyebi, A.; Pekin, B.K.; Pijanowski, B.C.; Plourde, J.D.; Doucette, J.S.; Braun, D. Hierarchical modeling of urban growth across the conterminous USA: Developing meso-scale quantity drivers for the Land Transformation Model. *J. Land Use Sci.* **2013**, *8*, 422–442. [CrossRef]
17. Mishra, V.N.; Rai, P.K.; Mohan, K. Prediction of land use changes based on land change modeler (LCM) using remote sensing: A case study of Muzaffarpur (Bihar), India. *J. Geogr. Inst. Jovan Cvijic SASA* **2014**, *64*, 111–127. [CrossRef]
18. Liu, X.; Liang, X.; Li, X.; Xu, X.; Ou, J.; Chen, Y.; Li, S.; Wang, S.; Pei, F. A future land use simulation model (FLUS) for simulating multiple land use scenarios by coupling human and natural effects. *Landsc. Urban Plan.* **2017**, *168*, 94–116. [CrossRef]
19. Qiang, Y.; Lam, N.S. Modeling land use and land cover changes in a vulnerable coastal region using artificial neural networks and cellular automata. *Environ. Monit. Assess.* **2015**, *187*, 57. [CrossRef]
20. Abdullahi, S.; Pradhan, B. Sustainable brownfields land use change modeling using GIS-Based weights-of-evidence approach. *Appl. Spat. Anal. Policy* **2016**, *9*, 21–38. [CrossRef]
21. Abdullahi, S.; Pradhan, B.; Mojaddadi, H. City compactness: Assessing the influence of the growth of residential land use. *J. Urban Technol.* **2018**, *25*, 21–46. [CrossRef]
22. Mustafa, A.; Rienow, A.; Saadi, I.; Cools, M.; Teller, J. Comparing support vector machines with logistic regression for calibrating cellular automata land use change models. *Eur. J. Remote Sens.* **2018**, *51*, 391–401. [CrossRef]
23. Zhang, Y.; Luo, J.; Zhang, Y.; Huang, Y.; Cai, X.; Yang, J.; Mao, D.; Li, J.; Tuo, X.; Zhang, Y. Resolution Enhancement for Large-Scale Real Beam Mapping Based on Adaptive Low-Rank Approximation. *IEEE Trans. Geosci. Remote Sens.* **2022**, *60*, 1–21. [CrossRef]
24. Wang, P.; Yu, P.; Lu, J.; Zhang, Y. The mediation effect of land surface temperature in the relationship between land use-cover change and energy consumption under seasonal variations. *J. Clean. Prod.* **2022**, *340*, 130804. [CrossRef]
25. Zhang, S.; Bai, X.; Zhao, C.; Tan, Q.; Luo, G.; Wang, J.; Li, Q.; Wu, L.; Chen, F.; Li, C. Global CO_2 consumption by silicate rock chemical weathering: Its past and future. *Earth's Future* **2021**, *9*, e2020EF001938. [CrossRef]
26. Xu, L.; Liu, X.; Tong, D.; Liu, Z.; Yin, L.; Zheng, W. Forecasting urban land use change based on cellular automata and the PLUS model. *Land* **2022**, *11*, 652. [CrossRef]
27. Liu, X.; Kong, M.; Tong, D.; Zeng, X.; Lai, Y. Property rights and adjustment for sustainable development during post-productivist transitions in China. *Land Use Policy* **2022**, *122*, 106379. [CrossRef]
28. Tong, D.; Chu, J.; Han, Q.; Liu, X. How land finance drives urban expansion under fiscal pressure: Evidence from Chinese cities. *Land* **2022**, *11*, 253. [CrossRef]
29. Liu, X.; Li, Z.; Fu, X.; Yin, Z.; Liu, M.; Yin, L.; Zheng, W. Monitoring House Vacancy Dynamics in The Pearl River Delta Region: A Method Based on NPP-VIIRS Night-Time Light Remote Sensing Images. *Land* **2023**, *12*, 831. [CrossRef]
30. Liu, Z.; Xu, J.; Liu, M.; Yin, Z.; Liu, X.; Yin, L.; Zheng, W. Remote sensing and geostatistics in urban water-resource monitoring: A review. *Mar. Freshw. Res.* **2023**. [CrossRef]
31. Sun, R.; Fu, L.; Cheng, Q.; Chiang, K.-W.; Chen, W. Resilient Pseudorange Error Prediction and Correction for GNSS Positioning in Urban Areas. *IEEE Internet Things J.* **2023**. [CrossRef]
32. Liu, Y.; Zhang, K.; Li, Z.; Liu, Z.; Wang, J.; Huang, P. A hybrid runoff generation modelling framework based on spatial combination of three runoff generation schemes for semi-humid and semi-arid watersheds. *J. Hydrol.* **2020**, *590*, 125440. [CrossRef]
33. Xu, D.; Zhu, D.; Deng, Y.; Sun, Q.; Ma, J.; Liu, F. Evaluation and empirical study of Happy River on the basis of AHP: A case study of Shaoxing City (Zhejiang, China). *Mar. Freshw. Res.* **2023**. [CrossRef]
34. Zhao, X.; Wang, P.; Yasir, M.; Liu, Z. Decision support system based on spatial and temporal pattern evolution of ecological environmental quality in the Yellow River Delta from 2000 to 2020. *Soft Comput.* **2022**, *26*, 11033–11044. [CrossRef]

35. Liang, X.; Guan, Q.; Clarke, K.C.; Liu, S.; Wang, B.; Yao, Y. Understanding the drivers of sustainable land expansion using a patch-generating land use simulation (PLUS) model: A case study in Wuhan, China. *Comput. Environ. Urban Syst.* **2021**, *85*, 101569. [CrossRef]
36. Lu, C.; Qi, X.; Zheng, Z.; Jia, K. PLUS-model based multi-scenario land space simulation of the Lower Yellow River Region and its ecological effects. *Sustainability* **2022**, *14*, 6942. [CrossRef]
37. Lin, Z.; Peng, S. Comparison of multimodel simulations of land use and land cover change considering integrated constraints-A case study of the Fuxian Lake basin. *Ecol. Indic.* **2022**, *142*, 109254. [CrossRef]
38. Bao, S.; Yang, F. Spatio-temporal dynamic of the land use/cover change and scenario simulation in the southeast coastal shelterbelt system construction project region of China. *Sustainability* **2022**, *14*, 8952. [CrossRef]
39. Yang, W.; Du, J.; He, H.; Yang, W.; Chen, L. Urban growth boundary delimitation in Guangzhou city based on PLUS-UGB multi-scenarios simulation. *Geospat. Inf* **2022**, *20*, 38–42.
40. Gao, L.; Tao, F.; Liu, R.; Wang, Z.; Leng, H.; Zhou, T. Multi-scenario simulation and ecological risk analysis of land use based on the PLUS model: A case study of Nanjing. *Sustain. Cities Soc.* **2022**, *85*, 104055. [CrossRef]
41. Li, X.; Fu, J.; Jiang, D.; Lin, G.; Cao, C. Land use optimization in Ningbo City with a coupled GA and PLUS model. *J. Clean. Prod.* **2022**, *375*, 134004. [CrossRef]
42. Wang, J.; Zhang, J.; Xiong, N.; Liang, B.; Wang, Z.; Cressey, E.L. Spatial and temporal variation, simulation and prediction of land use in ecological conservation area of Western Beijing. *Remote Sens.* **2022**, *14*, 1452. [CrossRef]
43. Rumelhart, D.E.; Hinton, G.E.; Williams, R.J. Learning representations by back-propagating errors. *Nature* **1986**, *323*, 533–536. [CrossRef]
44. Yu, Y.; Si, X.; Hu, C.; Zhang, J. A review of recurrent neural networks: LSTM cells and network architectures. *Neural Comput.* **2019**, *31*, 1235–1270. [CrossRef]
45. Xu, T.; Zhou, D.; Li, Y. Integrating ANNs and Cellular Automata–Markov Chain to Simulate Urban Expansion with Annual Land Use Data. *Land* **2022**, *11*, 1074. [CrossRef]
46. Boulila, W.; Ghandorh, H.; Khan, M.A.; Ahmed, F.; Ahmad, J. A novel CNN-LSTM-based approach to predict urban expansion. *Ecol. Inform.* **2021**, *64*, 101325. [CrossRef]
47. Wang, H.; Zhao, X.; Zhang, X.; Wu, D.; Du, X. Long time series land cover classification in China from 1982 to 2015 based on Bi-LSTM deep learning. *Remote Sens.* **2019**, *11*, 1639. [CrossRef]
48. Mohanrajan, S.N.; Loganathan, A. Novel vision transformer–based bi-LSTM model for LU/LC prediction—Javadi Hills, India. *Appl. Sci.* **2022**, *12*, 6387. [CrossRef]
49. Yang, J.; Huang, X. The 30 m annual land cover dataset and its dynamics in China from 1990 to 2019. *Earth Syst. Sci. Data* **2021**, *13*, 3907–3925. [CrossRef]
50. Hochreiter, S.; Schmidhuber, J. Long short-term memory. *Neural Comput.* **1997**, *9*, 1735–1780. [CrossRef]
51. Tsokos, C.P.; Welch, R. Bayes discrimination with mean square error loss. *Pattern Recognit.* **1978**, *10*, 113–123. [CrossRef]
52. Perica, S.; Foufoula-Georgiou, E. Model for multiscale disaggregation of spatial rainfall based on coupling meteorological and scaling descriptions. *J. Geophys. Res. Atmos.* **1996**, *101*, 26347–26361. [CrossRef]
53. Pontius, R.G.; Boersma, W.; Castella, J.-C.; Clarke, K.; De Nijs, T.; Dietzel, C.; Duan, Z.; Fotsing, E.; Goldstein, N.; Kok, K. Comparing the input, output, and validation maps for several models of land change. *Ann. Reg. Sci.* **2008**, *42*, 11–37. [CrossRef]